Science Advances
AAAS

Supplementary Materials for

Bias-preserving gates with stabilized cat qubits

Shruti Puri*, Lucas St-Jean, Jonathan A. Gross, Alexander Grimm, Nicholas E. Frattini, Pavithran S. Iyer, Anirudh Krishna, Steven Touzard, Liang Jiang, Alexandre Blais, Steven T. Flammia, S. M. Girvin

*Corresponding author. Email: shruti.puri@yale.edu

The PDF file includes:

> Supplementary Methods
> Supplementary Text
> Figs. S1 to S5
> References

1 Noise frequency at which leakage out of the cat manifold is possible

Suppose the oscillator couples to the environment with a general operator,

$$\hat{O} = \sum_{m,n} \chi_{m,n}(t) e^{i\omega_{\rm r}(m-n)t} \hat{a}^{\dagger m} \hat{a}^n + \text{h.c}, \tag{S1}$$

which is written in a frame rotating at the resonance frequency $\omega_{\rm r}$ of the oscillator. In the interaction picture of $\hat{H}_0(\phi) = -K\hat{a}^{\dagger 2}\hat{a}^2 + P(\hat{a}^{\dagger 2}e^{2i\phi} + \hat{a}^2 e^{-2i\phi})$,

$$\hat{\tilde{O}} = \sum_{m,n} \chi_{m,n}(t) e^{i\omega_{\rm r}(m-n)t} e^{i\hat{H}_0 t} \hat{a}^{\dagger m} \hat{a}^n e^{-i\hat{H}_0 t} + \text{h.c} \tag{S2}$$

If the oscillator started in one of the cat states, then the rate of leakage to the $p^{\rm th}$ excited state is,

$$\langle \psi_{\rm e,p}^{\pm} | \hat{\tilde{O}} | \mathcal{C}_\alpha^{\pm} \rangle = \sum_{m,n} \chi_{m,n}(t) e^{i\omega_{\rm r}(m-n)t} e^{-i(E_0 - E_{\rm e,p}^{\pm})t} \langle \psi_{\rm e,p}^{\pm} | \hat{a}^{\dagger m} \hat{a}^n | \mathcal{C}_\alpha^{\pm} \rangle$$
$$+ \sum_{m,n} \chi_{m,n}(t) e^{i\omega_{\rm r}(n-m)t} e^{-i(E_0 - E_{\rm e,p}^{\pm})t} \langle \psi_{\rm e,p}^{\pm} | \hat{a}^{\dagger n} \hat{a}^m | \mathcal{C}_\alpha^{\pm} \rangle \tag{S3}$$

Clearly $\langle \psi_{\rm e,p}^{\pm} | \hat{\tilde{O}} | \mathcal{C}_\alpha^{\pm} \rangle$ can be resonant when the spectral density of $\chi_{m,n}(t)$ is non-zero at $\omega_{\rm r}(m - n) - (E_0 - E_{\rm e,p}^{\pm})$ or $\omega_{\rm r}(n - m) - (E_0 - E_{\rm e,p}^{\pm})$. To elaborate with an example, if $m = 1, n = 0$ and α is large so that $E_0 - E_{\rm e,1}^+ \sim E_0 - E_{\rm e,1}^- \sim 4K\alpha^2$ then the resonant transition to the first excited manifold happens when the frequency of noise at $\omega_{\rm r} - 4K\alpha^2$ is non-zero.

2 White frequency noise

Coupling with a white dephasing channel leads to the Lindbladian master equation,

$$\dot{\hat{\rho}} = -i[\hat{H}_0(\phi), \hat{\rho}] + \kappa_\phi \mathcal{D}[\hat{a}^\dagger a]\hat{\rho}. \tag{S4}$$

In the above expression, κ_ϕ is the dephasing rate. Following the approach used in the manuscript to analyze the effect of white thermal noise, we describe the dynamics of the oscillator in the quantum-jump formalism. In this approach evolution under a non-Hermitian Hamiltonian $\hat{H} = \hat{H}_0(\phi) - i\kappa_\phi \hat{a}^\dagger \hat{a}\hat{a}^\dagger \hat{a}/2$ is interrupted by stochastic quantum jumps corresponding to the operators $\hat{a}^\dagger \hat{a}$. Again, for $\kappa_\phi \ll |\Delta\omega_{\rm gap}|$, the leading order effect of the non-Hermitian terms in $\hat{H}$ is to broaden the linewidths of the eigenstates of the oscillator. Action of $\hat{a}^\dagger \hat{a}$ on a state in the cat subspace causes leakage to $\mathcal{C}_\perp$. In the limit of large α, $\hat{a}^\dagger \hat{a} | \mathcal{C}_\alpha^{\pm} \rangle \sim \alpha^2 | \mathcal{C}_\alpha^{\pm} \rangle + \alpha | \psi_{\rm e,1}^{\pm} \rangle$ (note that the parity does not change). Therefore, a dephasing event excites the first excited subspace at rate $\sim \kappa_\phi \alpha^2$. As we saw in the last section, if a two-photon dissipation channel is introduced
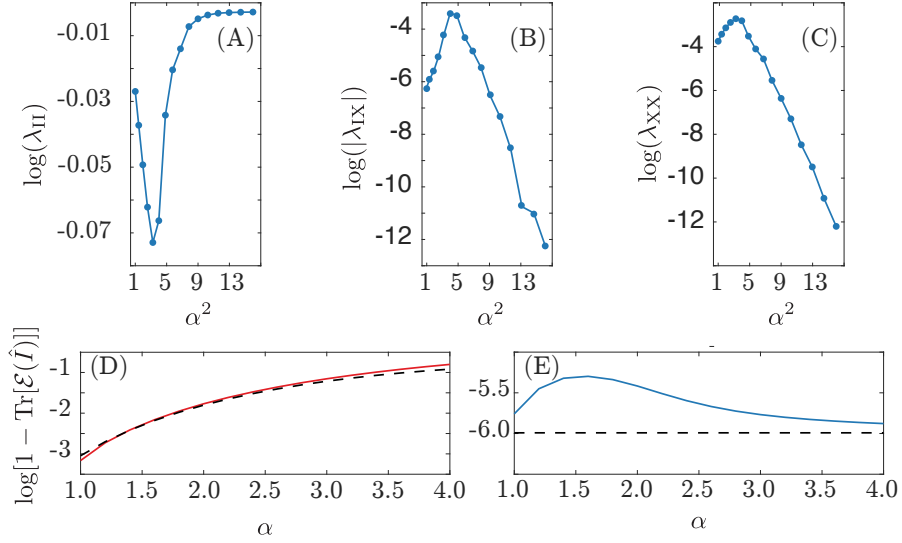
Figure S1: **Noise channel of the cat-qubit in the presence of white frequency noise. (A,B,C)** Natural logarithm of the coefficients of the error channel of an idle cat qubit in the presence of white dephasing noise and two-photon dissipation. As expected the amount of non-phase errors decreases exponentially with α^2. The parameters for the simulations are $\kappa_\phi = K/1000$ and $\kappa_{2\mathrm{ph}} = K/10$. The coefficients are evaluated at $t = 50/K$. **(D,E)** Natural logarithm of the amount of leakage, $\log[1 - \mathrm{Tr}[\mathcal{E}(\hat{I})]]$ in the presence of white dephasing noise without two-photon dissipation (red solid line in (D)) and with it (blue solid line in (E)). As expected, the two-photon dissipation autonomously corrects for leakage. The dashed black line shows the leakage predicted by the theoretical expressions for the rates of out-of-subspace excitations ($\sim \kappa_\phi \alpha^2$) and correction due to two-photon loss $\sim 4\kappa_{2\mathrm{ph}}\alpha^2$. These expression are only approximations which become more and more exact as α increases.

then the leakage will be corrected at a rate $4\kappa_{2ph}\alpha^2$. As a result, leakage errors are suppressed by $\sim \kappa_\phi/4\kappa_{2ph}$.

Observe that both dephasing and two-photon loss events cause transitions within the same parity subspace. Therefore, two-photon loss immediately after a dephasing event does not result in phase-flips. As a result, no phase-flips are introduced but bit-flips can arise because of the energy difference between the states $|\psi_{e,1}^{\pm}\rangle$. However, the energy difference and consequently the probability of a bit-flip, decreases exponentially with α^2 and the noise bias is preserved. The analysis above is confirmed by numerically simulating the master equation,

$$\dot{\rho} = -i[\hat{H}_0(\phi_0), \hat{\rho}] + \kappa_\phi \mathcal{D}[\hat{a}^\dagger \hat{a}]\hat{\rho} + \kappa_{2ph}\mathcal{D}[\hat{a}^2]\hat{\rho}. \tag{S5}$$

The dissipation rates κ_{2ph} and κ_ϕ are fixed, while α is varied by changing $\hat{H}_0(\phi)$ where

$$\hat{H}_0(\phi_0) = -K\hat{a}^{\dagger 2}\hat{a}^2 + P(\hat{a}^{\dagger 2}e^{2i\phi_0} + \text{h.c.}), \tag{S6}$$

$$2\phi_0 = \tan^{-1}(\kappa_{2ph}/2K), \quad P = \alpha^2 \sqrt{K^2 + \frac{\kappa_2^2}{4}}. \tag{S7}$$

The error channel is of the form

$$\mathcal{E}(\hat{\rho}) = \lambda_{II}\hat{I}\hat{\rho}\hat{I} + \lambda_{IX}\hat{I}\hat{\rho}\hat{X} + \lambda_{IX}^*\hat{X}\hat{\rho}\hat{I} + \lambda_{XX}\hat{X}\hat{\rho}\hat{X}. \tag{S8}$$

Figure S1(A,B,C) shows the numerically evaluated coefficients λ_{II}, λ_{IX}, and λ_{XX} at time $t = 50/K$ for $\kappa_\phi = K/1000$ and $\kappa_{2ph} = K/10$. All other coefficients cause a change in parity and hence are zero. As expected for large α, the bit-flips and consequently $|\lambda_{IX}|$ and λ_{XX} decrease exponentially with α^2. Figure S1(D,E) shows the amount of leakage $1 - \text{Tr}[\mathcal{E}(\hat{I})]$ with and without the two-photon dissipation. When $\alpha \to 0$, the cat states $|\mathcal{C}_0^{\pm}\rangle$ are the vacuum and single-photon Fock state respectively. In this case, frequency jumps do not cause any leakage because the vacuum and single-photon Fock states are eigenstates of $\hat{a}^\dagger \hat{a}$. Therefore, in the limit of small α, the leakage and consequently $|\lambda_{IX}|$ and λ_{XX} increase as α increases. Once α becomes sufficiently large, the exponential suppression of bit-flips with increase in α begins. The behavior in the limits of small and large α explains the trend in $|\lambda_{IX}|$ and λ_{XX} (and hence also λ_{II}) shown in Fig. S1(A,B,C). Figure S1(D,E) shows the numerically and theoretically estimated leakage. The theoretical estimation uses the expression $\kappa_\phi \alpha^2$ for the rate of leakage and $4\kappa_{2ph}\alpha^2$ for the rate of autonomous correction. We find that the theoretically predicted leakage is a good approximation for the numerically simulated leakage.

3   Threshold for imperfect rotation

In this section, we will first provide a qualitative estimate for the threshold of rotation error $\Delta_{th} \sim 0.5$ in the CX gate. We then provide a numerical estimate for the threshold which is in good agreement with the qualitative result.
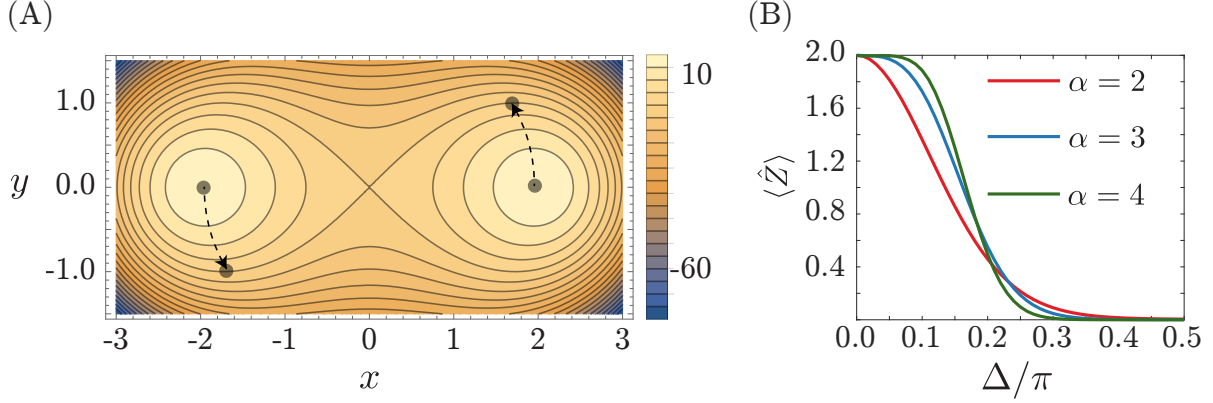
(A)

(B)

Figure S2: **Threshold for imperfect rotation.** **(A)** The meta potential of the Hamiltonian on the two-photon driven nonlinear oscillator, $f(x,y) = -K(x^2 + y^2)^2 + 2K\alpha^2(x^2 - y^2)$. The dark lines are the lines of equi-potential $f(x,y) = $ const. or the trajectories along which a classical particle moves. Since the nonlinearity if negative, the motion of the particle is clockwise. The trajectories for which $f(x,y) < 0$ are closed around $\pm\alpha$, while they are delocalized for $f(x,y) \geq 0$. At equilibrium the particle is at one of the two semiclassical stable points $(x,y) = (\pm\alpha, 0)$, shown in grey circles. A rotation error with $\Delta = \pi/3$ places the particle on the first delocalized path $f(x,y) = 0$. **(B)** $\langle \hat{Z} \rangle$ as a function of the rotation error Δ for different α at $t = 2/\kappa_2$ for $\kappa_2 = K/100$. The initial state of the oscillator is rotated by Δ, that is $\hat{Z} \to e^{i\hat{a}^\dagger \hat{a}} \hat{Z} e^{-i\hat{a}^\dagger \hat{a}}$. Two photon dissipation is added to refocus the rotated state back into the cat basis. Non-dephasing errors can be introduced during this correction process which would decrease $\langle \hat{Z} \rangle$. However, as expected from analytics, the numerical simulations show a thresholding behavior. That is, the $\hat{Z}$ decreases less rapidly for larger α for small Δ. The plot suggests a thresholding behaviour around $\Delta \sim 0.5$.

To begin with, consider a single cat-qubit in a two-photon driven nonlinear oscillator. We work in the limit of large α, so that the computational states $|0, 1\rangle$ are well approximated by the coherent states $| \pm \alpha \rangle$. Now suppose that the oscillator is initialized in a coherent state $e^{i\Delta\hat{a}^\dagger \hat{a}}|\alpha\rangle = |e^{i\Delta}\alpha\rangle$ or $e^{i\Delta\hat{a}^\dagger \hat{a}}| - \alpha \rangle = | - e^{i\Delta}\alpha\rangle$. These are not computational states, but as we have seen before, addition of two-photon dissipation will bring them back into the computational basis. Our task is to find the threshold Δ_{th} so that for $\Delta < \Delta_{\text{th}}$ the initial state $e^{i\Delta\hat{a}^\dagger \hat{a}}|\alpha\rangle$ evolves preferably to $|\alpha\rangle$ instead of $| - \alpha\rangle$, while the state $e^{i\Delta\hat{a}^\dagger \hat{a}}| - \alpha\rangle$ evolves (exponentially) preferably to $| - \alpha\rangle$ instead of $|\alpha\rangle$. Consequently, for $\Delta < \Delta_{\text{th}}$ phase-flips will be exponentially suppressed. It is reasonable to assume that the threshold obtained in this manner is identical to that for the rotation error in the CX gate.

Consider the master equation of such an oscillator in the presence of two-photon dissipation,

$$\dot{\rho} = -i[\hat{H}_0(\phi_0), \hat{\rho}] + \kappa_{2\text{ph}}\mathcal{D}[\hat{a}^2]\hat{\rho}. \tag{S9}$$

Using $\langle \hat{a} \rangle = x + iy$, in the semiclassical approximation

$$\dot{x} = 2Ky[\alpha^2 + (x^2 + y^2)] - \kappa_2 x[\alpha^2 - (x^2 + y^2)]$$
$$\dot{y} = 2Kx[\alpha^2 - (x^2 + y^2)] + \kappa_2 y[\alpha^2 + (x^2 + y^2)]. \tag{S10}$$

The equations of motion have the form of a particle moving on a metapotential or phase-space potential. For $K \gg \kappa_2$, the metapotential is $f(x, y) = -K(x^2 + y^2)^2 + 2K\alpha^2(x^2 - y^2)$, which is an inverted double well in the phase-space with peaks at $\pm\alpha$ (41,42). Figure S2(A) shows the contour plot of the metapotential. In semiclassical approximation, these contours are the trajectories along which a particle moves (clockwise because the nonlinearity is attractive.) The trajectories corresponding to $f(x, y) < 0$ are closed around $\pm\alpha$ and for $f(x, y) \geq 0$ they are delocalized. The state of the oscillator $|e^{i\Delta}\alpha\rangle$ or $|-e^{i\Delta}\alpha\rangle$ is equivalent to the particle being at $(x_0, y_0) = (\alpha\cos(\Delta), \alpha\sin(\Delta))$ or $(x_0, y_0) = (-\alpha\cos(\Delta), -\alpha\sin(\Delta))$ in the semiclassical approximation. If Δ is small, then (x_0, y_0) lies on one of the closed trajectories around $\pm\alpha$. Whereas, for large Δ, (x_0, y_0) lies on one of the delocalized trajectories. If the semiclassical trajectory is closed, then under the influence of quantum fluctuations and two-photon jumps, the initial states $|\pm e^{i\Delta}\alpha\rangle$ evolve preferably to $|\pm\alpha\rangle$ respectively. However, if the phase-space path is delocalized, then the initial states $|\pm e^{i\Delta}\alpha\rangle$ will evolve equally likely to either $|\alpha\rangle$ or $|-\alpha\rangle$. The threshold Δ_{th} is then the rotation angle such that $\alpha e^{i\Delta}$ lies on the first of delocalized trajectory $f(x, y) = 0$. Thus, solving the equation $f(\alpha\cos(\Delta), \alpha\sin(\Delta)) = 0$ gives the threshold $\Delta_{\text{th}} = \pi/6 \sim 0.52$. This semiclassical estimate of the threshold is valid in the regime $K \gg \kappa_2$. In the opposite regime $\kappa_2 \gg K$ the threshold is $\sim \pi/2$ (17). In the intermediate regime where κ_2 and K are of similar magnitudes, we expect the threshold to be between $\pi/6$ and $\pi/2$.

To justify this simple analysis of we numerically simulate the master equation,

$$\dot{\hat{\rho}} = -i[\hat{H}(\phi_0), \hat{\rho}] + \kappa_2 \mathcal{D}[\hat{a}^2]\hat{\rho} \tag{S11}$$

with $\hat{H}(\phi_0) = -K\hat{a}^{\dagger 2}\hat{a}^2 + P(\hat{a}^{\dagger 2}e^{2i\phi_0} + \hat{a}^2 e^{-2i\phi_0})$, $P = \alpha^2\sqrt{K^2 + \kappa_2^2/4}$ and $2\phi_0 = \tan^{-1}(\kappa_2/2K)$. The input state at $t = 0$ is $\exp(i\Delta\hat{a}^\dagger\hat{a})\hat{Z}\exp(-i\Delta\hat{a}^\dagger\hat{a})$, where $\hat{Z}$ is the Pauli operator $\hat{Z} = |0\rangle\langle 0| - |1\rangle\langle 1| = |\mathcal{C}_\alpha^+\rangle\langle \mathcal{C}_\alpha^-| + |\mathcal{C}_\alpha^-\rangle\langle \mathcal{C}_\alpha^+|$. From the simulations we estimate $\langle \hat{Z} \rangle$ at time $t = 2/\kappa_2$, $\kappa_2 = K/100$ for different α and Δ. As shown in Figure S2(B), the dependence of $\langle \hat{Z} \rangle$ as a function of Δ for different α suggests a thresholding behaviour around $\Delta \sim 0.5$. The figure shows that the numerical result does agree qualitatively with the analytic prediction. The large Hilbert space size limits the numerical simulations for larger α.

4 Geometric and topological phases during the CX gate

As described in the main text, the rotation of cat states in phase space along a closed loop gives rise to both geometric and topological phase. The topological phase arises simply because the state $|\mathcal{C}_\beta^-\rangle$ is 2π periodic in the phase of β, while the state $|\mathcal{C}_\beta^+\rangle$ has the periodicity of π. The

geometric or Berry phase *(43)* depends only on the path in the phase space. The difference in this phase for the two cat states is related to the mean particle number difference. Near $\beta = 0$ the state $|\mathcal{C}_\beta^+\rangle$ becomes the vacuum and the state $|\mathcal{C}_\beta^-\rangle$ becomes the single-photon Fock state, so that the photon number difference is 1. However for large β, the mean photon numbers for the two cat states become exponentially close. In phase space where $x = (\beta + \beta^*)/2$ and $x = (\beta - \beta^*)/2$, the Berry phase for the states $|\mathcal{C}_\alpha^\pm\rangle$ can be defined using the corresponding Berry connection as *(44,45)*,

$$\Phi_{\mathrm{g}}^\pm = \int A_x^\pm dx + A_y^\pm dy \tag{S12}$$

where,

$$A_x^\pm = \tfrac{1}{2}\left(\frac{1 \mp e^{-2(x^2+y^2)}}{1 \pm e^{-2(x^2+y^2)}}\right) y, \quad A_y^\pm = -\frac{1}{2}\left(\frac{1 \mp e^{-2(x^2+y^2)}}{1 \pm e^{-2(x^2+y^2)}}\right) x \tag{S13}$$

The corresponding Berry curvatures are,

$$\Omega^\pm = \frac{\partial A_y^\pm}{\partial x} - \frac{\partial A_x^\pm}{\partial y} = -\frac{1 \mp e^{-2(x^2+y^2)}}{1 \pm e^{-2(x^2+y^2)}} \mp \frac{4(x^2+y^2)e^{-2(x^2+y^2)}}{(1 \pm e^{-2(x^2+y^2)})^2} \tag{S14}$$

The Berry curvature and connection can be thought of as a magnetic flux and an electromagnetic vector potential respectively. The difference in the Berry curvature or flux $\Omega^+ - \Omega^-$ is small near the origin and at large x, y or $|\beta|^2$. The difference in Berry connection or vector potential is large near the origin and decreases exponentially away from it. Therefore, as long as the $|\beta|^2$ is large enough so that the closed path in phase space is not too close to the origin, then the geometric phase difference between the $|\mathcal{C}_\alpha^+\rangle$ and $|\mathcal{C}_\alpha^-\rangle$ will be exponentially small. In this case, topology is the only source of phase difference between the $|\mathcal{C}_\alpha^+\rangle$ and $|\mathcal{C}_\alpha^-\rangle$ state. Consequently, for the topological implementation of the CX gate, the size of the cat state must be large.

5 Impossibility of universal set of bias-preserving gates at the level of physical qubits

Consider physical qubits with a biased noise channel such that dephasing errors are dominant over non-dephasing fault. Suppose that the set of gates $(U_1, U_2, ..., U_k)$ are universal and preserve the bias. This set of operations can be single- or multi-qubit gates. Since each U_i preserves the bias, $U_i \hat{Z}_m = f(\hat{Z}_1, \hat{Z}_2, ...)U_i$, where $\hat{Z}_m$ is the Pauli matrix for the mth qubit and $f(\hat{Z})$ is some function of $\hat{Z}$-matrices of some number of qubits. Since $(U_1, U_2, ..., U_k)$ is a set of universal gates, it should be possible to construct a Hadamard gate on the mth qubit, $H = \Pi_i U_i$. If this were true, then $H\hat{Z}_m = (\Pi_i U_i)\hat{Z}_m = f'(\hat{Z}_1, \hat{Z}_2, ...)\Pi_i U_i = f'(\hat{Z}_1, \hat{Z}_2, ...)H$. However, we know that $H\hat{Z}_m = \hat{X}_m H \neq f'(\hat{Z}_1, \hat{Z}_2, ...)H$ for any function f'. Clearly, this a contradiction showing that it is not possible to have a universal set of bias-preserving gates to begin with.
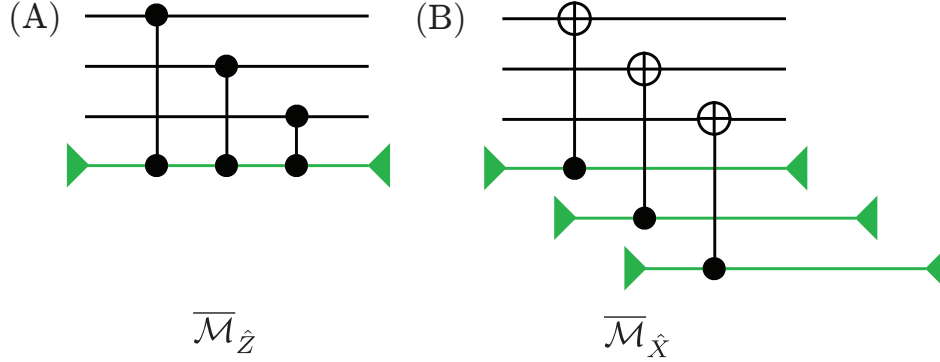
Figure S3: **Fault-tolerant gadgets for non-destructive measurements (A)** $\overline{\mathcal{M}}_{\hat{Z}}$ and **(B)** $\overline{\mathcal{M}}_{\hat{X}}$.

6 Clifford gadgets for the second-level encoding

The $\mathcal{C}_1$ protected $\mathcal{C}_2$ Clifford gadgets are $\{\overline{\text{CX}}, \overline{\mathcal{P}}_{|+\rangle}, \overline{\mathcal{P}}_{|0\rangle}, \overline{\mathcal{M}}_{\hat{Z}}, \overline{\mathcal{M}}_{\hat{X}}\}$. The $\overline{\text{CX}}$ gadget has been discussed in the main text. The rest of the gadgets are similar to ref. *(8)*. The scheme for non-destructive measurement $\overline{\mathcal{M}}_{\hat{Z}}$ is shown in Fig. S3(A). The ancilla is prepared in state $|+\rangle$ and CZ gates are implemented between the ancilla and each qubit in the repetition code. Finally, the ancilla is measured along the X-axis. For fault-tolerance measurement with ancilla is repeated r times and $\hat{Z}_{\text{L}}$ is determined by a majority vote on the measurement outcome. Figure S3(B) shows the gadget $\overline{\mathcal{M}}_{\hat{X}}$. The non-destructive measurement of $\hat{Z}_{\text{L}}$ is carried out by performing transversal measurement of $\hat{Z}$ on each qubit in the repetition code. For measuring $\hat{Z}$ on each qubit, a CX gate is realized between the qubit and an ancilla prepared in $|+\rangle$. The ancilla is then measured along $\hat{X}$. For fault-tolerance, each $\hat{Z}$ measurement is repeated r times and taking the majority of the outcome. The state $|+\rangle_{\text{L}}$ can be prepared transversally by preparing each cat qubit in the $|\mathcal{C}_\alpha^+\rangle$ state. The preparation $|0\rangle_{\text{L}}$ proceeds by first preparing $|+\rangle_{\text{L}}$ and then performing non-destructive measurement of $\hat{Z}_{\text{L}}$.

7 Bias-preserving CCX using only three-wave mixing

One can generalize the CX Hamiltonian, given in the main text, to a Hamiltonian for a controlled-controlled-NOT (CCX) gate—also known as a Toffoli gate—by adding a term to stabilize the second control oscillator and adapting the terms $(\beta \pm \hat{a}_{\text{c}})/2\beta$ (and their conjugates) to more involved expressions

$$\frac{\beta - \hat{a}_{\text{c}}}{2\beta} \rightarrow \frac{1}{4}\left(1 - \frac{\hat{a}_{\text{c1}}}{\beta} - \frac{\hat{a}_{\text{c2}}}{\gamma} + \frac{\hat{a}_{\text{c1}}\hat{a}_{\text{c2}}}{\beta\gamma}\right) \tag{S15}$$

$$\frac{\beta + \hat{a}_{\text{c}}}{2\beta} \rightarrow \frac{1}{4}\left(3 + \frac{\hat{a}_{\text{c1}}}{\beta} + \frac{\hat{a}_{\text{c2}}}{\gamma} - \frac{\hat{a}_{\text{c1}}\hat{a}_{\text{c2}}}{\beta\gamma}\right), \tag{S16}$$
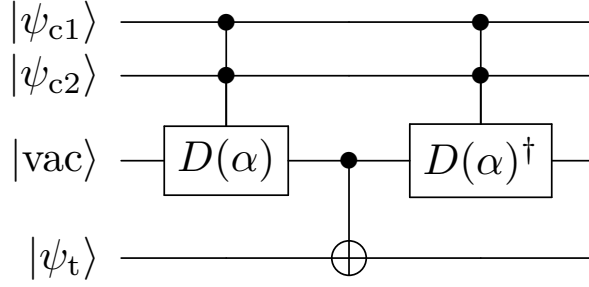
Figure S4: **Implementation of CCX using the CCD gate.**

where $\hat{a}_{\mathrm{c1}}$ and $\hat{a}_{\mathrm{c2}}$ are the annihilation operators for the two control oscillators, with stabilized subspaces defined by the coherent-state amplitudes β and γ. This direct implementation of a CCX is undesireable, though, because it requires interaction terms that are quartic in the creation and annihilation operators arising from the cross terms between the above expressions and the two-photon drive of the target oscillator. We instead propose to implement a CCX in a less direct manner that only requires interaction terms cubic in the creation and annihilation operator. We accomplish this through the use of an ancillary oscillator and a three-body entangling gate that only requires cubic interaction terms and using the ancillary oscillator as the control for a final CX.

The three-body gate we propose is the controlled-controlled displacement (CCD) gate. The Hamiltonian for the gate is

$$
\hat{H}_{\mathrm{CCD}}(t) = -K\left(\hat{a}_{\mathrm{c1}}^{\dagger 2} - \beta^2\right)\left(\hat{a}_{\mathrm{c1}}^2 - \beta^2\right) - K\left(\hat{a}_{\mathrm{c2}}^{\dagger 2} - \gamma^2\right)\left(\hat{a}_{\mathrm{c2}}^2 - \gamma^2\right) - K\left(\hat{a}_{\mathrm{t}}^{\dagger 2} - \alpha(t)^2\right)\left(\hat{a}_{\mathrm{t}}^2 - \alpha(t)^2\right)
$$

$$
- \delta\left[\hat{a}_{\mathrm{t}}^\dagger - \alpha(t)\frac{1}{2}\left(1 + \frac{\hat{a}_{\mathrm{c1}}^\dagger}{\beta} + \frac{\hat{a}_{\mathrm{c2}}^\dagger}{\gamma} - \frac{\hat{a}_{\mathrm{c1}}^\dagger\hat{a}_{\mathrm{c2}}^\dagger}{\beta\gamma}\right)\right]\left[\hat{a}_{\mathrm{t}} - \alpha(t)\frac{1}{2}\left(1 + \frac{\hat{a}_{\mathrm{c1}}}{\beta} + \frac{\hat{a}_{\mathrm{c2}}}{\gamma} - \frac{\hat{a}_{\mathrm{c1}}\hat{a}_{\mathrm{c2}}}{\beta\gamma}\right)\right]
$$

$$
+ i\dot{\alpha}(t)\left(\hat{a}_{\mathrm{t}}^\dagger - \hat{a}_{\mathrm{t}}\right)\frac{1}{2}\left(1 + \frac{\hat{a}_{\mathrm{c1}} + \hat{a}_{\mathrm{c1}}^\dagger}{2\beta} + \frac{\hat{a}_{\mathrm{c2}} + \hat{a}_{\mathrm{c2}}^\dagger}{2\gamma} - \frac{(\hat{a}_{\mathrm{c1}} + \hat{a}_{\mathrm{c1}}^\dagger)(\hat{a}_{\mathrm{c2}} + \hat{a}_{\mathrm{c2}}^\dagger)}{2\beta\gamma}\right),
$$

$$
\text{(S17)}
$$

where $\alpha(t)$ adiabatically transitions from $\alpha(0) = 0$ at the beginning of the gate to $\alpha(T) = \alpha$ by the end of the gate.

This gate displaces the target oscillator from vacuum at $t = 0$ to $|-\alpha\rangle \approx |1\rangle$ at $t = T$ if both control oscillators are in $|1\rangle$, otherwise it displaces the target to $|\alpha\rangle$. By applying this gate from two controls to an ancilla prepared in vacuum, applying a CX from the ancilla to the ultimate target, and unentangling the ancilla by applying the inverse of the displacement gate (see Fig S4), an effective CCX is applied from the two controls to the ultimate target without the need for any quartic interaction terms.

In the computational subspace the gate effects the isometry

$$\text{CCD} : |00\rangle \mapsto |000\rangle \tag{S18}$$
$$|01\rangle \mapsto |001\rangle \tag{S19}$$
$$|10\rangle \mapsto |010\rangle \tag{S20}$$
$$|11\rangle \mapsto |111\rangle . \tag{S21}$$

To show that the evolution given by Eq. (S17) results in a bias-preserving CCD, we perform simulations equivalent to those described for the CX gate. A Schrödinger-equation simulation of the three oscillators, with $\alpha = \beta = \gamma = 2$, $\delta = K/2$, $\alpha(t) = t/T$, and $T = 10/K$, yields an average-gate infidelity with the ideal CCD gate of 1.42×10^{-5}.

To simulate the master equation evolution in the presence of loss, we simplify the bath for the two control oscillators such that the spectral density of its thermal photons are narrow, allowing us to approximate them as qubits with effective Lindblad operators given by Eq. (11) and Eq. (12) in the main text. The target oscillator is simulated as evolving in the presence of a thermal bath with a white-noise spectrum.

Using the same Hamiltonian parameters as for the Schrödinger-equation simulation and setting the error-channel parameters to $\kappa = K/4000$ and $n_{\text{th}} = 1\%$ yields an average-gate fidelity of 98%. The leakage due to thermal photons in this case is $\sim 1.5 \times 10^{-5}$, and the bias is $\eta_{\text{CCD}} \sim 2500$. We also simulate adding two-photon dissipation for the gate time T after the gate has completed, with $\kappa_2 = K/5$, as a means of reducing the leakage. In this case, the leakage is reduced by almost an order of magnitude $\sim 2 \times 10^{-6}$, at the cost of reducing the average-gate fidelity to 96% and the bias to $\eta_{\text{CCD}} \sim 2300$.

In calculating leakage and bias for the CCD gate there are some subtleties due to the isometric nature of the gate. The process matrix is most naturally constructed as a map from operators on the domain of the gate (the subspace of inputs to the gate) to operators on the range of the gate (the subspace spanned by all outputs of the gate), restricted to the computational subspace of the oscillators. For all processes, the coefficient for the mapping from identity on the domain to identity on the codomain (the vector space the gate maps into, which can generally be larger than the range) tells how much of the trace is preserved when restricting to the computational subspace. For unitaries, this is the same as the coefficient mapping from identity on the domain to identity on the range, since the range equals the codomain. For isometries, this is not the case, and the coefficient mapping identity on the domain to identity on the range does not capture how much trace is retained in the computational subspace. In the particular case of the CCD gate, when restricting to the computational subspaces of the oscillators, the range is the 4-dimensional subspace spanned by $\{|000\rangle, |001\rangle, |010\rangle, |111\rangle\}$, while the codomain is the 8-dimensional subspace spanned by all 3-bit strings. Errors in the gate implementation can map input operators into operators with support outside of the range but still within the codomain, and we must be careful to not count these errors as leakage. It is important then to explicitly take the image of the computational-identity input in the whole oscillator space and project on the computational subspace (the codomain) in order to properly account for how much trace is preserved, and therefore how much leakage occurs.

The bias calculation is complicated because one does not probe all inputs to a 3-qubit error channel. This is because the states in the range of an ideal CCD cannot distinguish between certain distinct error processes in the computational subspace. It is cumbersome to express the indistinguishable error processes for the CCD gate, so for clarity consider the simpler CD gate

$$\text{CD} : |0\rangle \mapsto |00\rangle \tag{S22}$$
$$|1\rangle \mapsto |11\rangle . \tag{S23}$$

This gate is also an isometry, mapping to a range that is a 2-dimensional subspace of a 4-dimensional codomain. The range consists of states of the form $c_0|00\rangle + c_1|11\rangle$. Because of the symmetry of these states, IZ and ZI errors have exactly the same effect, so as far as the CD gate is concerned these error processes are equivalent. To characterize the inequivalent errors in our implementation, it is useful to look at the images of errors on the input states. For the CD gate, a Z error on the input has the same effect as either an IZ or a ZI error on the output. So for the CD gate, one can determine the probability of a dephasing-type error occurring on the output by computing the probability of a dephasing error occurring at the input. This ensures that a ZZ error on the output is correctly ignored, since on the range ZZ acts like the identity.

Similarly, for the CCD gate, one determines that the probability of a dephasing error occurring on the output is equal to the probability of a IZ, ZI, or ZZ error occurring on the input. The probability of other errors occurring is the probability of staying in the computational subspace, minus the probability of the II action and the dephasing errors. The bias is then calculated as the ratio of these two probabilities.

8   Magic-state preparation

In this section, we extend the analysis in *(10)* for the preparation of magic states $\bar{\mathcal{P}}_{|i\rangle}$ and $\bar{\mathcal{P}}_{|\text{T}\rangle}$. The gadget for magic state preparation is shown in Fig. S5 (A). The gadget consists of two repetition code blocks initialized in the state $|+\rangle_\text{L}$. The non-Clifford operation in this gadget is the transversal application of $ZZ(\theta)$ gates between the physical qubits in block 1 and block 2. The transversally applied $ZZ(\theta)$ gates do not preserve the codespace and this operation is not equivalent to a logical $\overline{ZZ}(\theta)$ gate. Following this step, a $\overline{\mathcal{M}}_{\hat{Z}}$ measurement is performed on block 1, followed by $\overline{\mathcal{M}}_{\hat{X}}$ measurement which disentangles block 1 from block 2. Finally, error correction is performed on block 2 to map it into the codespace. We will now elaborate how this gadget leads to a deterministic preparation of $|i\rangle_\text{L}$ state and probabilistic preparation of $|\text{T}\rangle_\text{L}$ with appropriate choice of θ.

After blocks 1 and 2 are each prepared in the $|+\rangle_\text{L} = |+\rangle^{\otimes n}$ state, the pairwise $ZZ(\theta)$ gates entangles them. The state after the application of this operation is

$$|\psi\rangle = [|0\rangle|\theta\rangle + \hat{X}\hat{X}|0\rangle|\theta\rangle]^{\otimes n}, \tag{S24}$$

where $|\theta\rangle = \cos(\theta/2)|+\rangle + i\sin(\theta/2)|-\rangle$. The $\overline{\mathcal{M}}_{\hat{Z}}$ measurement on block 1 projects it in a state with even or odd number of $|1\rangle$ depending on the measurement outcome $\overline{\mathcal{M}}_{\hat{Z}} = 1$ or
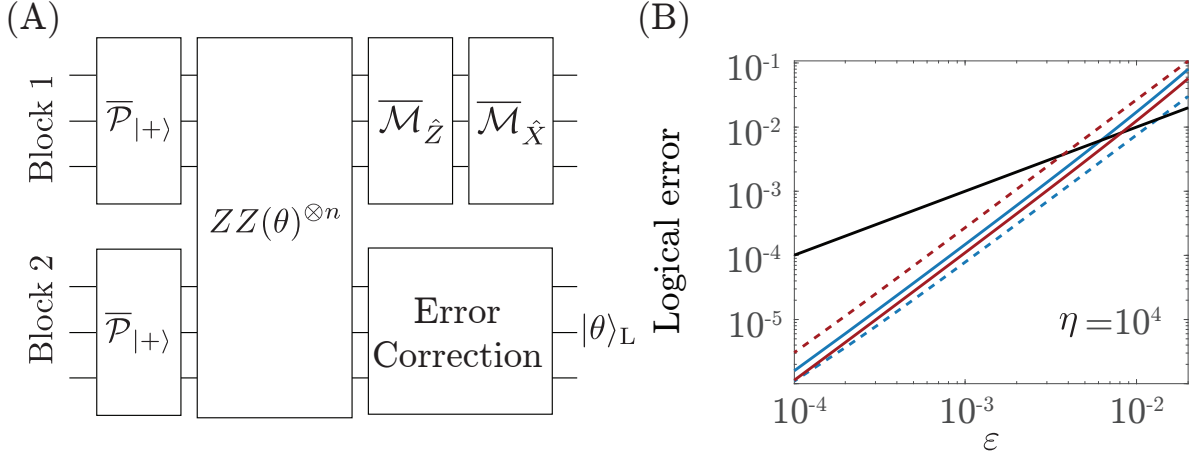
Figure S5: **Magic state distillation. (A)** Scheme for magic state preparation adapted from *(10)*. The error-correction gadget used is shown in Fig. (4) in the main text. **(B)** Logical dephasing and non-dephasing error rate for state preparation given in Eq. (S36) (solid blue line) and Eq. (S32) (dashed blue line) using $n = r = r_{\mathrm{z,L}} = 3$. For comparion the logical dephasing and non-dephasing rates from ref. *(10)* are shown using solid and dashed red lines, respectively. The black line with slope=1 is shown for reference.

$\overline{\mathcal{M}}_{\hat{Z}} = -1$ respectively. The state of the system after the $\overline{\mathcal{M}}_{\hat{Z}}$ measurement is

$$|\psi\rangle^{\overline{\mathcal{M}}_{\hat{z}}=1} = \sum_{|a|=\mathrm{even}} \bigotimes_{i=1}^{n} (\hat{X}\hat{X})^{a_i}|0\rangle|\theta\rangle$$

$$|\psi\rangle^{\overline{\mathcal{M}}_{\hat{z}}=-1} = \sum_{|a|=\mathrm{odd}} \bigotimes_{i=1}^{n} (\hat{X}\hat{X})^{a_i}|0\rangle|\theta\rangle, \tag{S25}$$

where $a_i \in \{0,1\}$. To give an example, if $n = 3$, $|\psi\rangle^{\overline{\mathcal{M}}_{\hat{z}}=1} = |000\rangle_1 \otimes |\theta\theta\theta\rangle_2 + |011\rangle_1 \otimes \hat{I}\hat{X}\hat{X}|\theta\theta\theta\rangle_2 + |101\rangle_1 \otimes \hat{X}\hat{I}\hat{X}|\theta\theta\theta\rangle_2 + |110\rangle_1 \otimes \hat{X}\hat{X}\hat{I}|\theta\theta\theta\rangle_2$ and $|\psi\rangle^{\overline{\mathcal{M}}_{\hat{z}}=-1} = |111\rangle_1 \otimes \hat{X}\hat{X}\hat{X}|\theta\theta\theta\rangle_2 + |100\rangle_1 \otimes \hat{X}\hat{I}\hat{I}|\theta\theta\theta\rangle_2 + |010\rangle_1 \otimes \hat{I}\hat{X}\hat{I}|\theta\theta\theta\rangle_2 + |001\rangle_1 \otimes \hat{I}\hat{I}\hat{X}|\theta\theta\theta\rangle_2$. Here the subscripts $1, 2$ denote the blocks 1 and 2 respectively. Next, an $\overline{\mathcal{M}}_{\hat{X}}$ measurement is performed on block 1. That is, each qubit in block 1 is measured along the $\hat{X}$ axis and is projected onto either the $|\mathcal{C}_\alpha^+\rangle$ or $|\mathcal{C}_\alpha^-\rangle$ state. If $b_i = \pm 1$ represents the result of the measurement on the ith qubit, then the state of the qubits in block 2 is

$$|\psi\rangle_b^{\overline{\mathcal{M}}_{\hat{z}}=1} = \sum_{|a|=\mathrm{even}} \bigotimes_{i=1}^{n} (b_i\hat{X})^{a_i}|\theta\rangle = A_b^1|\theta\rangle^{\otimes n} \tag{S26}$$

$$|\psi\rangle_b^{\overline{\mathcal{M}}_{\hat{z}}=-1} = \sum_{|a|=\mathrm{odd}} \bigotimes_{i=1}^{n} (b_i\hat{X})^{a_i}|\theta\rangle = A_b^{-1}|\theta\rangle^{\otimes n}. \tag{S27}$$

Here $A_b^{\pm 1} = \sum_{|a|=\text{even/odd}} \bigotimes_{i=1}^n (b_i \hat{X})^{a_i}$ and $A_b^{-1} = \hat{X}^{\otimes n} A_b^1 = \hat{X}_{\text{L}} A_b^1$. Consequently, the state of block 2 when the result of the $\overline{\mathcal{M}}_{\hat{Z}}$ measurement is -1 differs from that when the measurement result is 1 simply by $\hat{X}_{\text{L}}$. Therefore, for fault-tolerance, this measurement is repeated $r_{\text{z,L}}$ times and a majority vote is taken over the measurement outcomes. The above expressions can be simplified to

$$|\psi\rangle_b^{\overline{\mathcal{M}}_{\hat{z}}=1} = \left[\cos\left(\frac{\theta}{2}\right)\right]^s \left[i\sin\left(\frac{\theta}{2}\right)\right]^{n-s} \bigotimes_{i=1}^n |\mathcal{C}_\alpha^{\text{sign}(b_i)}\rangle$$
$$+ \left[i\sin\left(\frac{\theta}{2}\right)\right]^s \left[\cos\left(\frac{\theta}{2}\right)\right]^{n-s} \hat{Z}_{\text{L}} \bigotimes_{i=1}^n |\mathcal{C}_\alpha^{\text{sign}(b_i)}\rangle \tag{S28}$$

$$|\psi\rangle_b^{\overline{\mathcal{M}}_{\hat{z}}=-1} = \hat{X}_{\text{L}} |\psi\rangle_b^{\overline{\mathcal{M}}_{\hat{z}}=1}, \tag{S29}$$

where s is the number of $+1$ in b. The above expressions show that block 2 is in a super-position of qubit states which are completely correlated and completely anti-correlated to the qubit states in block 1. To elaborate with an example, for $n = 3$ if the $\overline{\mathcal{M}}_{\hat{Z}}$ measurement yields 1 and if the $\overline{\mathcal{M}}_{\hat{X}}$ measurement yields $b = 1, 1, 1$ or $b = -1, -1, -1$ then the state of the qubits in block 2 is $\cos(\theta/2)^3 |\mathcal{C}_\alpha^+\rangle |\mathcal{C}_\alpha^+\rangle |\mathcal{C}_\alpha^+\rangle + (i\sin(\theta/2))^3 |\mathcal{C}_\alpha^-\rangle |\mathcal{C}_\alpha^-\rangle |\mathcal{C}_\alpha^-\rangle$. If the $\overline{\mathcal{M}}_{\hat{X}}$ measurement yields $b = 1, 1, -1$ or $b = -1, -1, 1$ then the state of the qubits in block 2 is $\cos(\theta/2)^2 i\sin(\theta/2) |\mathcal{C}_\alpha^+\rangle |\mathcal{C}_\alpha^+\rangle |\mathcal{C}_\alpha^-\rangle + (i\sin(\theta/2))^2 \cos(\theta/2) |\mathcal{C}_\alpha^-\rangle |\mathcal{C}_\alpha^-\rangle |\mathcal{C}_\alpha^+\rangle$. Finally, the error-correction step on block 2 using the gadget, shown in Fig.(4) in the main text, projects block 2 back into the codespace,

$$|\psi\rangle_b^{\overline{\mathcal{M}}_{\hat{z}}=1} = \hat{Z}_{\text{L}}^{H[s-(n+1)/2]} \times$$
$$\left\{ \left[\cos\left(\frac{\theta}{2}\right)\right]^s \left[i\sin\left(\frac{\theta}{2}\right)\right]^{n-s} |+\rangle_{\text{L}} + \left[i\sin\left(\frac{\theta}{2}\right)\right]^s \left[\cos\left(\frac{\theta}{2}\right)\right]^{n-s} |-\rangle_{\text{L}} \right\} \tag{S30}$$

$$|\psi\rangle_b^{\overline{\mathcal{M}}_{\hat{z}}=-1} = \hat{X}_{\text{L}} |\psi\rangle_b^{\overline{\mathcal{M}}_{\hat{z}}=1}, \tag{S31}$$

where $H[s - (n+1)/2]$ is the heaviside step function. The above expression shows that the resulting code state depends on the choice of θ and the intermediate measurement results. Using $\theta = \pi/2$, the state $|i\rangle_{\text{L}}$ is prepared (up to correctable Pauli rotations) irrespective of the measurement outcome. Moreover, if we find that if the error syndromes obtained from the measurement of the stabilizer generators do not agree with the $\overline{\mathcal{M}}_{\hat{Z}}$ measurement on block 1, then we reject the state on block 2. Using $\theta = \pi/4$, the state $|\text{T}\rangle_{\text{L}}$ is prepared (up to correctable Pauli rotations) only when $n - s = s \pm 1$ or $s = (n \pm 1)/2$. Out of all the 2^n possible measurement results, the number of outputs that result in the correct state is $\binom{n}{\frac{n+1}{2}} + \binom{n}{\frac{n-1}{2}}$. Therefore, the probability of successful $|\text{T}\rangle_{\text{L}}$ state preparation is, $p_{\text{success}} = 2^{1-n}\binom{n}{\frac{n-1}{2}}$. For example, with $n = 9$ or $n = 21$, $p_{\text{success}} = 0.49$ or 0.34 respectively. The probability of success decreases with

increasing n because the $ZZ(\theta)^{\otimes n}$ gates do not preserve the codespace. Next, we will examine the probability of logical error in the preparation of the states.

A   Upper bound on the probability of a logical non-dephasing error

A logical non-dephasing fault in block 2 can be due to a physical non-dephasing error during the $2nr$ CX gates in the error correction gadget or during any of the n $ZZ(\theta)$ gates. Moreover, a faulty $\overline{\mathcal{M}}_{\hat{Z}}$ measurement also leads to a non-dephasing error (see Eq. (S31)). This can happen due to a non-dephasing error in any of the n $ZZ(\theta)$ gates or any of the $nr_{\mathrm{z,L}}$ CZ gates. It can also result if a majority $m = (r_{\mathrm{z,L}} + 1)/2$ of the measurements are faulty (either due to dephasing faults in any one of the n CZ gates or the preparation and measurement of the ancilla.) Therefore, the probability of a logical non-dephasing error is upper bounded by

$$\varepsilon_{\mathrm{x,L}} \leq (2nr + 2n + nr_{\mathrm{z,L}})\frac{\varepsilon}{\eta} + \binom{r_{\mathrm{z,L}}}{\frac{r_{\mathrm{z,L}}+1}{2}}(n\varepsilon + 2\varepsilon)^{(r_{\mathrm{z,L}}+1)/2}. \tag{S32}$$

B   Upper bound on the probability of $\hat{Z}_{\mathrm{L}}$ error

A logical dephasing error in block 2 could result from the failure of the error-correction block to detect any error. This happens if there is a phase-flip error on all the n qubits in block 2. Each qubit i in block 2 can undergo a phase-flip during any one of the $2r$ CX gates, the $ZZ(\theta)$ gate, preparation and when the ith qubit in block 1 undergoes a phase flip. In block 1, a phase error on a qubit can occur during preparation, measurement, $ZZ(\theta)$ gate and any one of the $r_{\mathrm{z,L}}$ CZ gates. Additionally, a bit-flip error in the ancilla for $\overline{\mathcal{M}}_{\hat{Z}}$ measurement can also introduce correlated phase-flip errors in block 1, which then propagates to block 2. To estimate the upper bound, we assume that a non-dephasing fault in any of the $nr_{\mathrm{z,L}}$ CZ gates results in undetectable error in block 2. Therefore, the probability of a $\hat{Z}_{\mathrm{L}}$ error in block 2 due to failure of the error-correction gadget is

$$\begin{aligned}\varepsilon_{\mathrm{z,L}}^{(1)} &\leq ((2r+2)\varepsilon + (r_{\mathrm{z,L}}+3)\varepsilon)^n + nr_{\mathrm{z,L}}\frac{\varepsilon}{\eta} \\ &\leq (2r\varepsilon + r_{\mathrm{z,L}}\varepsilon + 5\varepsilon)^n + nr_{\mathrm{z,L}}\frac{\varepsilon}{\eta}.\end{aligned} \tag{S33}$$

In addition, correlated phase errors in block 1 and block 2 is another source of fault. Recall that if the error syndromes obtained from the measurement of the stabilizer generators do not agree with the $\overline{\mathcal{M}}_{\hat{Z}}$ measurement on block 1 then the state is rejected. Correlated phase errors in the ith qubit in blocks 1 and 2, would however be missed, leading to an incorrect preparation of the magic state. Such correlated errors could occur during the n $ZZ(\theta)$ gates (probability $\varepsilon_{\mathrm{zz}}$) or due to independent errors ε^2 occurring during preparation, measurement, $ZZ(\theta)$ gates or $r_{\mathrm{z,L}}$ CZ gates in the $\overline{\mathcal{M}}_{\hat{Z}}$ measurement. Therefore, the probability of an $\varepsilon_{\mathrm{z,L}}^{(2)}$ error due to correlated

phase errors is

$$\varepsilon_{\mathrm{z,L}}^{(2)} \leq n\varepsilon_{\mathrm{zz}} + n(r_{\mathrm{z,L}}\varepsilon + 3\varepsilon)(2r\varepsilon + 2\varepsilon). \tag{S34}$$

A final source of fault is the correlated errors in block 2 and stabilizer measurements themselves. If a qubit in block 2 undergoes a phase-flip and if the stabilizers are measured correctly, then a comparison between block 1 and 2 will reveal this error and the state can be discarded. However, if the two stabilizer generators involving that qubit are measured incorrectly, then the error in block 2 will be missed. An upper bound on the probability for this fault path is

$$\varepsilon_{\mathrm{z,L}}^{(3)} \leq n(2r\varepsilon + r_{\mathrm{z,L}}\varepsilon + 5\varepsilon) \left(\binom{r}{\frac{r+1}{2}}(4\varepsilon)^{\frac{r+1}{2}} \right)^2. \tag{S35}$$

Finally, the total probability of a $\varepsilon_{\mathrm{z,L}}$ error is obtained by combining Eq. (S33), Eq. (S34) and Eq. (S35),

$$\begin{aligned}
\varepsilon_{\mathrm{z,L}} \leq{}& nr_{\mathrm{z,L}}\frac{\varepsilon}{\eta} + (2r\varepsilon + r_{\mathrm{z,L}}\varepsilon + 5\varepsilon)^n + n\varepsilon_{\mathrm{zz}} + n(r_{\mathrm{z,L}}\varepsilon + 3\varepsilon)(2r\varepsilon + 2\varepsilon) \\
&+ n(2r\varepsilon + r_{\mathrm{z,L}}\varepsilon + 5\varepsilon) \left(\binom{r}{\frac{r+1}{2}}(4\varepsilon)^{\frac{r+1}{2}} \right)^2.
\end{aligned} \tag{S36}$$

We can now compare the expressions for the logical error rates in Eq. (S32) and Eq. (S36) to those in *(10)*. Recall that the only difference in the preparation schemes described here is the error correction gadget based on stabilizer measurements using CX gates. This does not affect the leading order sourced of error, which is correlated phase-flips in block 1 and 2 ($\propto \varepsilon_{\mathrm{zz}}, \varepsilon^2$). The main difference is due to the contribution of correlated errors in block 2 and syndrome measurements (Eq. (S35)) to a logical $\hat{Z}_{\mathrm{L}}$ error. In contrast, faults due to measurement errors in the error-correction gadget used in Ref. *(10)* contribute to a logical $\hat{X}_{\mathrm{L}}$ error and are of higher order (see Eq. (17) in *(10)*). Figure S5(B) shows the logical error rates computed here and that from Ref. *(10)* for $n = r = r_{\mathrm{z,L}} = 3$. As expected, the probability of non-dephasing error with the CX based error-correction is slightly lower than in Ref. *(10)*, while the probability of dephasing errors is similar. In the previous section, we found that for $\eta = 10^4$, $\varepsilon = 0.0043$, and $n = 19$, $\varepsilon_{\mathrm{cat}} = 0.67 \times 10^{-3}$, which is the accuracy threshold for a CSS code. According to Eq. (S36) and Eq. (S32), the logical error probability in the preparation of the magic states when $\eta = 10^4$, $\varepsilon = 0.0043$, and $n = 19$ is 0.016, which is lower than the threshold for state distillation *(1,46)*.

REFERENCES AND NOTES

1. P. Aliferis, D. Gottesman, J. Preskill, Accuracy threshold for postselected quantum computation. *Quant. Inf. Comput.* **8**, 181–244 (2008).

2. E. Knill, Quantum computing with realistically noisy devices. *Nature* **434**, 39–44 (2005).

3. R. Raussendorf, J. Harrington, K. Goyal, Topological fault-tolerance in cluster state quantum computation. *New J. Phys.* **9**, 199 (2007).

4. I. M. Pop, K. Geerlings, G. Catelani, R. J. Schoelkopf, L. I. Glazman, M. H. Devoret, Coherent suppression of electromagnetic dissipation due to superconducting quasiparticles. *Nature* **508**, 369–372 (2014).

5. M. D. Shulman, O. E. Dial, S. P. Harvey, H. Bluhm, V. Umansky, A. Yacoby, Demonstration of entanglement of electrostatically coupled singlet-triplet qubits. *Science* **336**, 202–205 (2012).

6. T. Watson, S. G. J. Philips, E. Kawakami, D. R. Ward, P. Scarlino, M. Veldhorst, D. E. Savage, M. G. Lagally, M. Friesen, S. N. Coppersmith, M. A. Eriksson, L. M. K. Vandersypen, A programmable two-qubit quantum processor in silicon. *Nature* **555**, 633–637 (2018).

7. G. Waldherr, Y. Wang, S. Zaiser, M. Jamali, T. Schulte-Herbrüggen, H. Abe, T. Ohshima, J. Isoya, J. F. Du, P. Neumann, J. Wrachtrup, Quantum error correction in a solid-state hybrid spin register. *Nature* **506**, 204–207 (2014).

8. P. Aliferis, J. Preskill, Fault-tolerant quantum computation against biased noise. *Phys. Rev. A* **78**, 052331 (2008).

9. P. Aliferis, F. Brito, D. P. DiVincenzo, J. Preskill, M. Steffen, B. M. Terhal, Fault-tolerant computing with biased-noise superconducting qubits: A case study. *New J. Phys.* **11**, 013061 (2009).

10. P. Webster, S. D. Bartlett, D. Poulin, Reducing the overhead for quantum computation when noise is biased. *Phys. Rev. A* **92**, 062309 (2015).

11. A. Robertson, C. Granade, S. D. Bartlett, S. T. Flammia, Tailored codes for small quantum memories. *Phys. Rev. Applied* **8**, 064004 (2017).

12. D. K. Tuckett, S. D. Bartlett, S. T. Flammia, Ultrahigh error threshold for surface codes with biased noise. *Phys. Rev. Lett.* **120**, 050505 (2018).

13. D. K. Tuckett, A. S. Darmawan, C. T. Chubb, S. Bravyi, S. D. Bartlett, S. T. Flammia, Tailoring surface codes for highly biased noise. *Phys. Rev. X* **9**, 041031 (2019).

14. J. Guillaud, M. Mirrahimi, Repetition cat-qubits for fault-tolerant quantum computation. *Phys. Rev. X* **9**, 041053 (2019).

15. S. Puri, S. Boutin, A. Blais, Engineering the quantum states of light in a Kerr-nonlinear resonator by two-photon driving. *npj Quantum Inf.* **3**, 18 (2017).

16. N. Ofek, A. Petrenko, R. Heeres, P. Reinhold, Z. Leghtas, B. Vlastakis, Y. Liu, L. Frunzio, S. M. Girvin, L. Jiang, M. Mirrahimi, M. H. Devoret, R. J. Schoelkopf, Extending the lifetime of a quantum bit with error correction in superconducting circuits. *Nature* **536**, 441–445 (2016).

17. Z. Leghtas, S. Touzard, I. M. Pop, A. Kou, B. Vlastakis, A. Petrenko, K. M. Sliwa, A. Narla, S. Shankar, M. J. Hatridge, M. Reagor, L. Frunzio, R. J. Schoelkopf, M. Mirrahimi, M. H. Devoret, Confining the state of light to a quantum manifold by engineered two-photon loss. *Science* **347**, 853–857 (2015).

18. S. Touzard, A. Grimm, Z. Leghtas, S. O. Mundhada, P. Reinhold, C. Axline, M. Reagor, K. Chou, J. Blumoff, K. M. Sliwa, S. Shankar, L. Frunzio, R. J. Schoelkopf, M. Mirrahimi, M. H. Devoret, Coherent oscillations inside a quantum manifold stabilized by dissipation. *Phys. Rev. X* **8**, 021005 (2018).

19. A. Grimm, N. E. Frattini, S. Puri, S. O. Mundhada, S. Touzard, M. Mirrahimi, S. M. Girvin, S. Shankar, M. H. Devoret, The Kerr-Cat Qubit: Stabilization, Readout, and Gates. *Nature* **584**, 205–209 (2020).

20. S. Puri, A. Grimm, P. Campagne-Ibarcq, A. Eickbusch, K. Noh, G. Roberts, L. Jiang, M. Mirrahimi, M. H. Devoret, S. M. Girvin, Stabilized cat in driven nonlinear cavity: A fault-tolerant error syndrome detector. *Phys. Rev. X* **9**, 041009 (2019).

21. H. Goto, Universal quantum computation with a nonlinear oscillator network. *Phys. Rev. A* **93**, 050301 (2016).

22. M. Mirrahimi, Z. Leghtas, V. V. Albert, S. Touzard, R. J. Schoelkopf, L. Jiang, M. H. Devoret, Dynamically protected cat-qubits: A new paradigm for universal quantum computation. *New J. Phys.* **16**, 045014 (2014).

23. J. Cohen, W. C. Smith, M. H. Devoret, M. Mirrahimi, Degeneracy-preserving quantum nondemolition measurement of parity-type observables for cat qubits. *Phys. Rev. Lett.* **119**, 060503 (2017).

24. Y. Y. Gao, B. J. Lester, Y. Zhang, C. Wang, S. Rosenblum, L. Frunzio, L. Jiang, S. M. Girvin, R. J. Schoelkopf, Programmable interference between two microwave quantum memories. *Phys. Rev. X* **8**, 021073 (2018).

25. R. C. Bialczak, R. McDermott, M. Ansmann, M. Hofheinz, N. Katz, E. Lucero, M. Neeley, A. D. O'Connell, H. Wang, A. N. Cleland, J. M. Martinis, $1/f$ flux noise in josephson phase qubits. *Phys. Rev. Lett.* **99**, 187006 (2007).

26. D. Sank, R. Barends, R. C. Bialczak, Y. Chen, J. Kelly, M. Lenander, E. Lucero, M. Mariantoni, A. Megrant, M. Neeley, P. J. J. O'Malley, A. Vainsencher, H. Wang, J. Wenner, T. C. White, T. Yamamoto, Y. Yin, A. N. Cleland, J. M. Martinis, Flux noise probed with real time qubit tomography in a josephson phase qubit. *Phys. Rev. Lett.* **109**, 067001 (2012).

27. D. F. Walls, G. J. Milburn, *Quantum Optics* (Springer Science & Business Media, 2007).

28. P. Aliferis, J. Preskill, Fibonacci scheme for fault-tolerant quantum computation. *Phys. Rev. A* **79**, 012332 (2009).

29. J. J. Wallman, J. Emerson, Noise tailoring for scalable quantum computation via randomized compiling. *Phys. Rev. A* **94**, 052325 (2016).

30. D. K. Tuckett, S. D. Bartlett, S. T. Flammia, B. J. Benjamin, Fault-tolerant thresholds for the surface code in excess of 5% under biased noise. *Phys. Rev. Lett.* **124**, 130501 (2020).

31. Y. Fujiwara, Ability of stabilizer quantum error correction to protect itself from its own imperfection. *Phys. Rev. A* **90**, 062304 (2014).

32. E. T. Campbell, A theory of single-shot error correction for adversarial noise. *Quant. Sci. Tech.* **4**, 025006 (2019).

33. V. N. Premakumar, H. Sha, D. Crow, E. Bach, R. Joynt, 2-designs and redundant syndrome extraction for quantum error correction. arXiv:1907.04497 [quant-ph] (10 July 2019).

34. A. Ashikhmin, C.-Y. Lai, T. A. Brun, Robust quantum error syndrome extraction by classical coding, in *2014 IEEE International Symposium on Information Theory* (IEEE, 2014), pp. 546–550.

35. A. Ashikhmin, C.-Y. Lai, and T. A. Brun, Correction of data and syndrome errors by stabilizer codes, in *2016 IEEE International Symposium on Information Theory* (IEEE, 2016), pp. 2274–2278.

36. A. Ashikhmin, C.-Y. Lai, and T. A. Brun, Quantum data syndrome codes. arXiv:1907.01393 [quant-ph] (2 July 2019)

37. J. R. Johansson, P. D. Nation, F. Nori, QuTiP: An open-source python framework for the dynamics of open quantum systems. *Comput. Phys. Commun.* **183**, 1760–1772 (2012).

38. N. E. Frattini, U. Vool, S. Shankar, A. Narla, K. M. Sliwa, M. H. Devoret, 3-wave mixing josephson dipole element. *Appl. Phys. Lett.* **110**, 222603 (2017).

39. N. E. Frattini, V. V. Sivak, A. Lingenfelter, S. Shankar, M. H. Devoret, Optimizing the nonlinearity and dissipation of a SNAIL parametric amplifier for dynamic range. *Phys. Rev. Applied* **10**, 054020 (2018).

40. S. Touzard, A. Kou, N. E. Frattini, V. V. Sivak, S. Puri, A. Grimm, L. Frunzio, S. Shankar, M. H. Devoret, Gated conditional displacement readout of superconducting qubits. *Phys. Rev. Lett.* **122**, 080502 (2019).

41. M. Dykman, *Fluctuating Nonlinear Oscillators: From Nanomechanics to Quantum Superconducting Circuits* (Oxford Univ. Press, 2012).

42. S. Puri, C. K. Andersen, A. L. Grimsmo, A. Blais, Quantum annealing with all-to-all connected nonlinear oscillators. *Nat. Commun.* **8**, 15785 (2017).

43. M. V. Berry, Quantal phase factors accompanying adiabatic changes. *Proc. R. Soc. Lond. A* **392**, 45–57 (1984).

44. S. Chaturvedi, M. S. Sriram, V. Srinivasan, Berry's phase for coherent states. *J. Phys. A* **20**, L1071 (1987).

45. S. M. Girvin, K. Yang, *Modern Condensed Matter Physics* (Cambridge Univ. Press, 2019).

46. S. Bravyi, A. Kitaev, Universal quantum computation with ideal clifford gates and noisy ancillas. *Phys. Rev. A* **71**, 022316 (2005).